Egypt. J. Chem. **Vol. 67,** No. 6 pp. 247 - 256 (2024)

Egyptian Journal of Chemistry

http://ejchem.journals.ekb.eg/

Fabrication of flexible dielectric materials with improved mechanical properties using silicone rubber and Cu-Al-Zn alloy

Salwa H. El-Sabbagh[a]*, Amira Nassar[b], A.A. Ward[c], Wael S. Mohamed[a], Doaa S Mahmoud[a]

[a]*Department of Polymers and Pigments, National Research Center, Cairo, Egypt*

[b]*Solid State Physics Department, Metal Physics Laboratory, National Research Centre, Dokki, Giza, Egypt*

[c]*Department of Microwave Physics and Dielectrics, National Research Center, Cairo, Egypt*

Abstract

Dielectric polymer composites have unusual properties that have significantly increased in a wide variety of applications. However, shape memory materials, which are a significant part of the category of smart materials, are substances that possess specific characteristics, namely, shape memory affect (SME) and pseudo -elasticity. SME has been examined using thermo-mechanical techniques. In this approach, silicone rubber (SiR) composites using Cu-Al-Zn alloy as fillers may be able to achieve a high permittivity and low dielectric loss. The purpose of this study is to explore the effect of Cu-Al-Zn alloy in particle form on the physical properties of silicone rubber. The results disclosed an improvement in stiffness and elasticity as well as dielectric properties of silicone rubber/Cu-Al-Zn alloy composites. The results showed lower hysteresis at higher Cu-Al-Zn alloy content. Further, the values of permittivity ε' and dielectric loss ε″ of the investigated composite were in case of using Cu-Al-Zn alloy. Besides, the SiR composites containing Cu-Al-Zn alloy have a promising insulating performance and can be used in electric insulation applications. Additionally, the values of conductivity of the SiR/ Cu-Al-Zn alloy composites vary from 10^{-13} to ~10^{-9} S cm^{-1}. This value is sufficient for these composites to exhibit electrostatic dissipation behaviour.

Keywords:Silicone rubber (SiR); Cu-Al-Zn *based alloy; rheology; physico-mechanical; dielectric properties; DSC;*

1. Introduction

A variety of shape memory materials have been developed, and these materials exhibit some novel performance, including sensoring (thermal, stress, or field), adaptive responses, large-stroke actuation, high damping and shape memory smart systems [1]. Smart materials and structures used in design mostly to the field of structural engineering, robotics, and aerospace due to which the demand for highly functional and light weight, adaptive system is continuously growing [1, 2]. Because of their force recovery capabilities, unique strain and pseudo-elastic effect (PE), and distinctive functional characteristics, many metal alloys and polymers demonstrate the shape memory effect (SME). Shape memory materials (SMMs) are one of the main constituents of intelligent/smart composites due to their typical properties, including the shape memory effect pseudo-elasticity or wide recoverable stroke (strain), substantial damping capacity, and adaptive properties that are caused by the reversible transitions of phases in the components [1, 2]. In this direction, Copper-Aluminum-Zinc (Cu-Al-Zn) alloy belongs to the family of shape memory alloys (SMAs) and silicone rubber was fabricated for efficient structure uses. The typical behavior of each of the both constitutive materials is well known. Cu-Al-Zn alloy is a member of the shape memory effect and super elasticity property family, making it a good candidate for composite materials and intelligent composite structures [3]. Silicone rubber is an elastomer, or rubber-like material, made of silicone polymers that also contain oxygen, carbon, and hydrogen. The siloxane backbone, also referred to as silicone-oxygen links, is consistently formed by its structure. Silicone rubber forms silicone-oxygen links popularly known as siloxane backbone [4]. Its structure exhibits hyper elasticity allowing large deformations without permanent set [5]. The elasticity of rubber after expansion (in either compression or tension) is its most crucial characteristic. Abrasion resistance, air and water impermeability, and ability to resist swelling in oil/solvents are just a few of the many other beneficial properties that elastomers possess in both static and dynamic conditions. These characteristics can be seen at higher, ambient, or lower temperatures. They are also largely maintained in a variety of climatic settings, including ozone-rich atmospheres [6]. Smart materials are classified as shape memory polymers (SMP) based on their material characteristics, but they have a wide range of uses and properties. The complex materials integration caused by the significant mismatch among the mechanical and physical characteristics of metals and polymers is an important barrier to the development of active/smart materials [7,8]. Both stress and temperature exhibit a hysteretic cycle, recovering its original shape after removal of the load and dissipating of energy. Silicone rubber is a notable elastomer in the rubber

*Corresponding author e-mail: salwa_elsabbagh@yahoo.com. (Salwa H. El-Sabbagh)
Receive Date: 26 October 2023, Revise Date: 13 November 2023, Accept Date: 26 November 2023
DOI: 10.21608/EJCHEM.2023.244813.8778

industry owing to its outstanding resistance to ozone, ultraviolet, oxygen, and chemicals, in addition to its excellent electrical characteristics and physical lifelessness. It is usually used to build industrial products like cables, bio-implants, sealants, and gaskets. SiR, however, they have weak mechanical characteristics, especially a low tensile strength. As a result, reinforcing fillers like fumed and precipitated silica are commonly used to reinforce mechanical goods, which is fantastic for rubber [9-12]. The technological qualities improve when inorganic fillers are replaced with organic ones [13, 14]. Polymers' physical properties are continuously altered by the adding filler, which also lowers the cost of device. Reduced production costs are always a driving force behind the addition of fillers to polymers, even after changes to their physical qualities. The industry and academic studies have shown an increased interest in particulate-filled polymers throughout time.

Aim of this research is to examine how the melt-mixing method would affect the dispersion of various Cu-Al-Zn-based alloy at various contents in silicone rubber and how the filler loading affects the silicone rubber vulcanizate's curing, mechanical, and swelling properties. Additionally, the effect of Cu-Al-Zn alloy on the dielectric properties of SiR-composites will be also discussed.

2. Materials and experimental methodology

2.1. Materials

Silicone rubber was provided by SONAX (Nubreg,, Germany). The plasters used to strengthen the SiR matrix were a Cu-Al-Zn alloy DEVARD's, LOBA CHEMIE PVT.LTD, Molecular Weight of Devarda alloy: 943.7 g/mol- Molecular Formula $Al_9Cu_{10}Zn$. The investigated alloy (Cu-Al-Zn) had a particle range of order 25 µm and containing mostly dendritic assembly. Average particle size of Cu-Al-Zn alloy ranged amid 9.497µm-23.62µm. Activators stearic acid (St Ac) and Zinc oxide (ZnO). They were provided by the Aldrich Company in Germany. Dicumyl peroxide is used as vulcanizing agent.

2.2. Preparation of Cu-Al-Zn alloy/SiR- vulcanizates

SiR was diverse with its several elements (Table 1) in a two-roll mill (width 300mm, width 470mm, abrasion ratio 1:1.4 and haste of measured roll 24 rpm) at a normal system. Activators zinc oxide, stearic acid and peroxide curing were added to the SiR former to combination of the Cu-alloy. Then, Cu-Al-Zn alloy was additional with diverse loadings (2.5, 5, 10 and 15 phr) treated with coupling agents (3-(Trimethoxysilyl) propyl methacrylate (TMSPM) was added to the final response) under cautious switch of temperature (scheme 1). Vulcanization was accepted out in only-daytime electrically heated van controlled hydraulic press at 152 ± 1°C and pressure 4MPa [15, 16, and 17] and the vulcanizates were ready in according with ASTMD3182-07(2012).

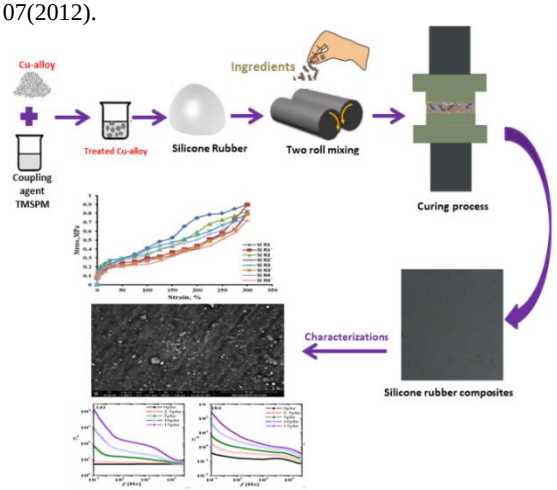

Scheme 1: The preparation process of silicone rubber composites

Table 1: Formulation, rheometric characteristics and Cu-Al-Zn alloy dispersion parameters of SiR vulcanizates at 152 °C

Cu-alloy content, phr*	CRI, min^{-1}	Tan δ	Renf. Ef.	η''_r	m''_r	L′
0 phr	25.2	0.029	---	---	---	--
2.5 phr	28.8	0.027	0.0078	1.08	1.012	0.068
5 phr	29.2	0.026	0.067	1.16	1.073	0.087
10 phr	28.7	0.025	0.0389	1.12	1.044	0.076
15 phr	29.5	0.226	0.0731	1.08	1.024	0.056

The Base recipe (in phr)* phr is part per hundred parts of rubber.: Silicone rubber (SiR) 100; stearic acid 2; zinc oxide 5; peroxide 3. Coupling agent 3-(Trimethoxysilyl) propyl methacrylate (TMSPM) 4; CRI: cure rate index; tanδ; the damping coefficient, Renf. Ef. Reinforcing efficiency for the fillers; $\eta''r$ the relative viscosity; $m''r$ the relative modulus, $L' = \eta''r - m''r$

2.3 Rheometric characteristics

The rheological characteristics of the silicone rubber containing variable quantities of Cu-Al-Zn alloy in the existence of pairing TMSPM factors were obvious using rheometer R-100 (MDR one Moving Die Rheometer, TA) at 152 ± 1°C rendering to ASTMD2084-11, 2011.

2.4 Mechanical properties

Stress, which was performed in accordance with ASTM D412-06a (2013), and strain at break were measured using a Zwick Roell Z010 tensile testing machine (Ulm, Germany). Five measurements were done for each sample, and the average value for each sample was then calculated.

2.5 Strain-energy determination

To calculate the strain energy, Simpson's rule was used [18, 19].

2.6 Measurement of swelling percentage

The swelling behavior of SiR loaded with different amounts of Cu-Al-Zn alloy- was carried out in toluene according to ASTM D471-16a (2021) .

2.7 Hysteresis loop area (HYS)

Hysteresis loss (HYS) is the quantity of energy dispersed through cyclic distortion and is computed using the area W_1 (work complete during extension) and W_2 (work done through regression) when the samples are stretched to a certain extent and then allowed to retract at the same rate to the un-stretched state:

$$HYS = W_1 - W_2 \qquad (1)$$

2.8 DSC analysis

The glass transition temperature of rubber composites was investigated using a differential scanning calorimeter (DSC) SDT-Q600, USA. The experiments were done under a nitrogen atmosphere at a heating rate of 10 °C/min from -150 °C to 260 °C.

2.9 Scanning electron microscopy (SEM*)*

The morphology of the prepared rubber composites were evaluated using a JEOL JX 840 micro-analyzer electron probe (Japan) for SEM examination.

2.10. Dielectric properties

Over a wide frequency range of 0.1 Hz to 1 MHz, the permittivity ε', dielectric loss ε" (where $\varepsilon'' = \varepsilon' * \tan\delta$,), tanδ; is the loss factor), and alternating resistance Rac were measured at room temperature (~ 30 °C). By connecting the impedance analyzer to a personal computer via a GPIB cable (IEEE488), the extent was computed. Data was acquired using a commercial interfacing and automation software called "Lab VIEW." The deviation in ε' and tan δ is around ±1% and ±3%, in that order. A temperature regulator equipped with a (Pt 100) sensor regulated the samples' temperature. The measurement error for temperature is ± 0.5 °C.

3. Results and Discussion

3.1.Rheological properties

The formulations and rheometric characteristics of SiR/Cu-alloy composites containing different concentrations of alloy in the presence of coupling agent (TMSPM) were collected in Table 1 and Figure 1(a &b). Adding Cu-Al-Zn alloy to SiR matrix slightly increased the minimum torque value (M_L), maximum torque (M_H) and torque difference (M_H - M_L). Where M_L was used to measure the mix's minimum viscosity and represented the composites' filler-filler interaggregate formation. The improvement in rheometric torque value is attributed to the leading rubber-alloy interaction, which intensifies with 15 phr alloy loading. The chain entanglements and crosslink density affect M_H. This outcome is explained by how the Cu-Al-Zn -alloy affects the crosslink density by reacting with the chemical constituents of the formulation, which results in a rising torque [17]. The optimum cure time values (tc_{90}) slightly decreased compared to their respective unfilled sample, this decrease is due to the introduction of Cu-Al-Zn alloy in different contents. With increase in the concentration of Cu-Al-Zn alloy, optimum cure time (tc90) values show a decrease in trend. This indicates that Cu-Al-Zn alloy/ TMSPM/peroxide accelerate the vulcanization process in these samples. This result is due to the formation of a transition metal complex in which peroxide and carbonyl ester groups(C=O) of intercalates may involve [20].

Also, the cure rate index (CRI) values of Cu-Al-Zn / Cu-Al-Zn alloy composites are high indicating that Cu-Al-Zn alloy has accelerating effect on the curing process, when compared with unfilled SiR samples. The damping coefficient tan δ at M_L obtained from the rheometric data is lower for the SiR/Cu-Al-Zn alloy composites as 15, 10, 5 and 2.5 phr Cu-Al-Zn alloy than SiR without filler. The Tanδ is directly related to crosslinking, and a smaller damping factor reveals a better crosslinking system [21].

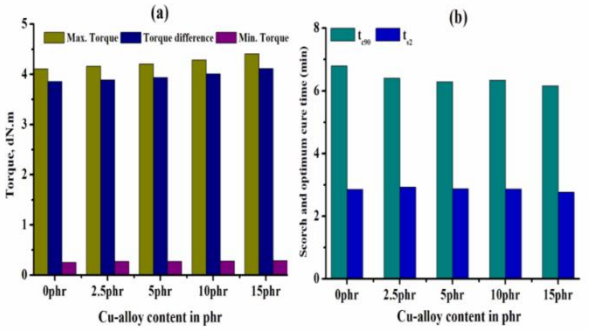

Figure 1: Rheometric characteristics of silicone rubber filled with various loading of Cu-Al-Zn alloy

3.2. Cu-Al-Zn alloy dispersion in SiR-valcanizates

The degree of filler dispersion with connecting agent in silicone rubber was quantitatively calculated by Lee [22–24] using the equation:

$$L = \eta_r'' - m_r'' \qquad (2)$$

The relative stickiness (η_r'') and the relative modulus (m_r'') could be determined from rheometric data, through the expressions.

$$\eta_r'' = \frac{M_L^{Cu}}{M_L^0} \text{ and } m_r'' = \frac{M_H''}{M_H^0} \qquad (3)$$

Where M_L , M_H means the torque minimum, and maximum and the superscripts, Cu and 0 relate to the filled and the unfilled silicone rubber, respectively.

Table 1 exhibits the intended η_r'' , m_r'', and L values, where it can be obviously seen that in case of mixes containing 15 phr of Cu-Al-Zn alloy in presence of coupling agent (TMSPM), the Cu-alloy elements are well scattered in the SiR matrix expect at lower loadings [15]. An increase Cu-Al-Zn alloy loading, the values η_r'' and m_r'', increased up to 10 phr, suggesting a rise in the elastomer's relative viscosity and modulus. However, at 15 phr of Cu-Al-Zn alloy loading the values of η_r'' or m_r'' decreased indicating a lower in relative viscosity and relative modulus of the elastomer. Furthermore, the greater the Cu-Al-Zn alloy dispersion in the silicone rubber matrix phase, the lower the value of L.

Furthermore, SiR composites with increased Cu- Al-Zn alloy loading show a larger difference in η_r'' or m_r'' values. In addition, the values of L decrease, where the lower the value of L the better is the Cu-Al-Zn alloy dispersion in the silicone rubber matrix phase. Moreover, at higher Cu-Al-Zn alloy loading in SiR composites, there is the higher difference between η_r'' and m_r'',

values. The index value L increases with Cu-Al-Zn alloy loading at 2.5, 5, 10 phr, indicating to the accumulation of the Cu-Al-Zn alloy in the SiR rubber matrix [15]. This description was in promise with the data in Table 1. The degree of strengthening of Cu-Al-Zn alloy in SiR template in the existence of prepared compatiblizer TMSPM was studied by Lee and Pal and De [19, 25 and 26]. The reinforcing efficiency (Renf.Ef.) was thoughtful by the next relation:

$$\text{Renf. Ef} = \frac{(M_H - M_L)_{Cu} - (M_H - M_L)_0}{(M_H - M_L)_0} \qquad (4)$$

Where M means the torque, the subscripts "Cu" and "0" are linked to the Cu-Al-Zn alloy and unloaded SiR. Table 1 shows the value of Renf Ef of Cu-Al-Zn alloy. High Rein forcing means high rubber / Cu-Al-Zn alloy interaction, which is affected by the amount of Cu-alloy distribution. It is obvious that presence of compatibilizer TMSPM caused a higher value of Rein. Ef for Cu-Al-Zn alloy (15 phr). This was due to well dispersion of Cu-Al-Zn alloy and a stronger interface of SiR in the existence of a compatibilizer. This description is in contract with the marks in Table 1.

3.3. Physical properties

The stress-strain curves are utilized to get an enhanced intelligence of how mechanical properties develop with several attentions to Cu-Al-Zn alloy loadings in all silicone rubber composites. From Figure. 2, these composites are sensitive to the condensations of the Cu-Al-Zn alloy contents. Moreover, for stated strain, each of filled schemes show rise stresses than unfilled rubber. It was found that there was an increasing tendency of strain (elongation) and stress (tensile strength) when the proportion of Cu-Al-Zn alloy was increased. This is because as alloy loading increases, cross-link density, or difference torque, progressively rises. The combination softened as more alloys were added, and as a result, elongation progressively rose. There is evidence that Cu-Al-Zn alloy has been added to SiR compounds by the conjugation factor (TMSPM), which creates additional physical cross-links in the composites' net structure. In the presence of 15 phr Cu-Al-Zn alloy into composites, higher levels of failure stress were observed. It was also observed that as the concentration of the alloy loadings rose, the samples' stiffness increased. Otherwise, this figure indicates that the addition of Cu-alloys resulted in a noticeable but minor increase in tensile strength, which suggests that the treated Cu-Al-Zn alloy/SiR (alloy/rubber) composites had better stiffness. Grounded on the obtained facts, it can be decided that the addition of Cu-alloy to rubber improves the physical properties and this is confirmed by the calculated strain energy.

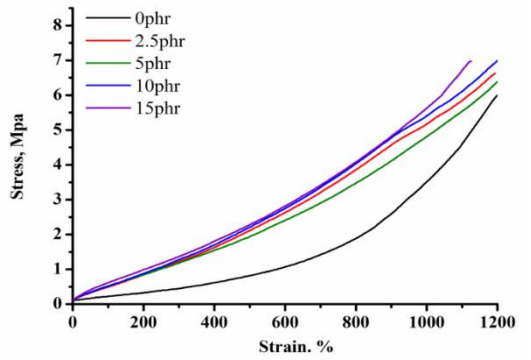

Figure 2: Stress-strain curves for the silicone rubber loading with different amounts of Cu-Al-Zn alloy

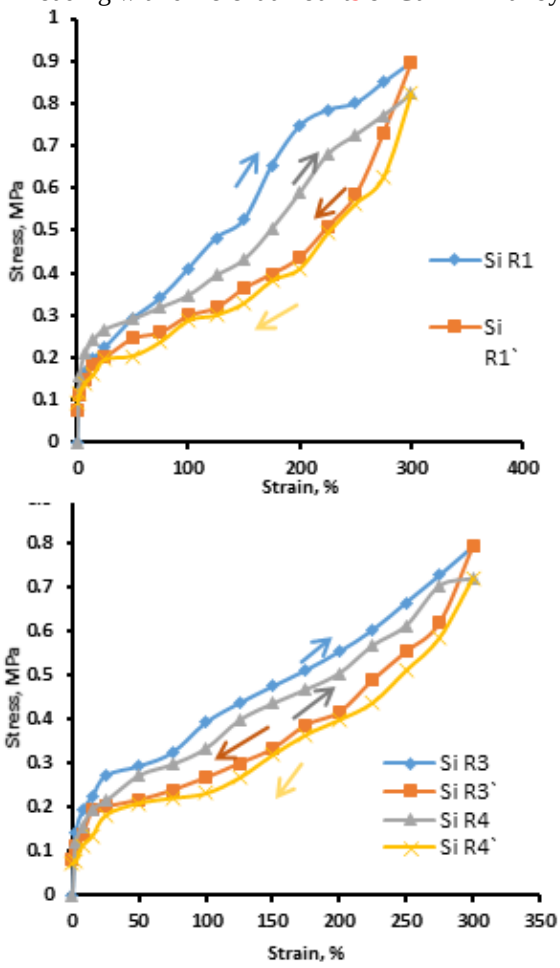

Figure 3: Hysteresis loop for the silicone rubber loading with different amounts of Cu-Al-Zn alloy

So, the energy absorbed per unit volume (En Ab) is predictable to increase in distorting silicone rubber composites. Thus the energy absorbed can be written as [27, 28]:

$$\text{En Ab} = \oint (\sigma\, \varepsilon)\, d\varepsilon \qquad (5)$$

Where σ is the stress at the function of strain ε; for that purpose, smaller energy absorption ability is a lower the area under the stress-strain curves. The composite contained 15 phr treated Cu-Al-Zn alloy/SiR has the lowest energy absorption of strain energy because it has

the smallest area under the stress-strain curve. Conversely, the highest energy absorption is found in silicone rubber loaded with different ratios of Cu-Al-Zn alloy, such as 2.5, 5 and 10 phr. These findings are in good contract with the facts presented in Table 2 and Figure 2. The decrease in the strain energy owing to the combination of 15 phr of Cu-Al-Zn alloy in SiR vulcanizes.

Table 2: Strain energy and the hysteresis loop area for first cycle of deformation to 300 % SiR/ Cu-Al-Zn alloy composites.

Samples	Strain energy, En Ab (MJ/m^3)	Hysteresis loop area (Hys) (MJ/m^3)
2.5phr	1.1492 x 10^3	41.312
5phr	1.1391 x 10^3	29.967
10phr	1.1733x 10^3	29.217
15phr	1.0758x 10^3	24.547

3.4. Impact of periodic stress-strain on mechanical properties

Stress relaxing or periodic distortions were performed for every treated Cu-Al-Zn alloy/SiR composites up to 300% of the elongation. Figure 3 depicts the hysteresis curves and, for all samples, the cyclic stress-strain curves at room temperature (25 + 273 K). Table 2 displays the hysteresis loop zone values for each SiR vulcanizates for the initial stress-strain cycle. These results demonstrate that the sample containing (15 phr Cu-Al-Zn alloy) had smaller hysteresis loop area Hys (24.547 MJ/m3) than other samples. This may perhaps ascribe to the rise of filler-matrix interactions by adding of Cu-Al-Zn alloy. The upper hysteresis loop area provides a sign of the amount of energy lack and therefore the heat build-up through the cyclic distortion [15, 19]. The smallest area indicates that stability of the composites SiR/ Cu-Al-Zn alloy, where Hys is reduced. Conversely, the part of energy that disperses will growth, resulting in a negative outcome, that is, higher heat buildup.

3.5. Swelling behavior of the Cu-Al-Zn alloy /SiR valcanizates

In order to explore the interaction between silicone rubber and the Cu-Al-Zn based alloy filler, some investigators adopted a swelling technique. Given that swelling can totally go away, adhesion may be the goal why Cu-Al-Zn alloy /SiR contact is constrained. The Lorenz and Parks equation [29-30] had been used to study SiR-filler interaction.

$$\frac{Eq_{Cu-alloy}}{Eq_{Si\,R}} = Ae^{-Z} + B \qquad (6)$$

Also, $$\frac{Eq_{Cu-allloy}}{Eq_{SiR}} = \frac{V_{r\,SiR}\,(1- V_{r\,Cu-alloy})}{V_{r\,Cu-alloy}\,(1-V_{r\,SiR})} \qquad (7)$$

Where Z is the ratio by weight of Cu-Al-Zn alloy to SiR hydrocarbon in the vulcanizate, and Eq is defined as grams of solvent per grams of hydrocarbon, and also, $V_{r\ Cu-alloy}$ is the volume fraction of the Cu-Al-Zn alloy filled SiR in the swollen gel, $V_{r\,SiR}$ is the pure gum. A & B are the constant.

So that,

$$\frac{V_{r\,Cu-alloy}}{V_{r\,SiR}} = A\,e^{-Z} + B \qquad (8)$$

Kranbuehl [23] claims that the value (1/Eq) can be utilized to calculate the effect of the interaction between SiR and Cu-Al-Zn alloy. Higher values of $(\frac{Eq_{Cu-allloy}}{Eq_{SiR}})$ resulted in less interaction between the Cu-Al-Zn alloy filler and the SiR matrix. The optimal ratio is 15 phr, whether there is a coupling agent presents (TMSPM). Data from Table 3 demonstrated that using 10 or 15 phr Cu-Al-Zn alloy produced the lowest value of $(\frac{Eq_{Cu-allloy}}{Eq_{SiR}})$ and the greatest value of (1/Eq), indicating a stronger SiR Rubber/ Cu-Al-Zn alloy interaction. These results are due to the formation of cross-links, which was strong-minded from equilibrium swelling amounts using the molecular weight between cross-links (Mc) in accordance with the Flory-Rehner connection equation [31].

Table 3 contains a list of the information exposed for crosslink density v increases with increasing alloy content up to 10 phr and then slightly decreases with increasing alloy content up to 15 phr, according to the sign vd in table 3. Additionally, the rubber volume portion (Vr) could be taken as an amount of reinforcing ability of the Cu-Al-Zn -based alloy [26, 32, and 33]. From Table 3, it could be seen that volume portion (Vr) values improved with adding the Cu-Al-Zn -based alloy and those all lie upper than the control samples (ophr) where no alloy was added. Table 3 shows that, by introducing metal as filler to SiR compounds, the Cu-Al-Zn alloy may be causing a swelling restriction in the silicone rubber (SiR) matrix.

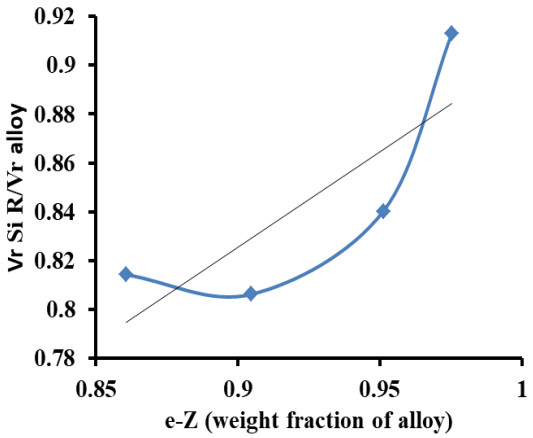

Figure 4: The change in Vr SiR/Vr alloy (volume fraction of pure and filled silicone rubber) with e-Z (Weight fraction of alloy)

The findings were supported by the relationship between volume fraction (Vr) of SiR Cu-Al-Zn alloy and e-z (weight fraction of alloy), which is illustrated in Figure. 4. The ratio of Vr SiR/Vr alloy shows the restriction of silicone rubber matrix swelling brought on by the presence of Cu-based alloy. These numbers demonstrated that because Vr of SiR is a constant, as alloy loading rises due to a reduction in the sample's solvent absorption, the ratio of Vr SiR to Cu-Al-Zn alloy decreases. It was clearly seen that, from Table 3, the value of (Eq Cu-alloy/Eq SiR) was decreasing with increasing Cu-alloy loading. Greatest probably, the surface-surface interaction was stronger in the case of

higher loaded Cu-Al-Zn alloy composites. The lowest value of Eq. Cu-Al-Zn alloy/Eq SiR was obtained at 10 and also 15 phr of alloy loading. This reveals that the furthest filler–filler interaction was found at the highest loading of Cu-Al-Zn alloy (15 phr).

Table 3: The influence of treated Cu-Al-Zn alloy/SiR composites on the swelling properties

Sample	Eq, %	Vr	$\nu_{d\ ,(mol/cm^3)}$	Mwc, (g mol^{-1})	$\frac{Eq_{Cu-alloy}}{Eq_{SiR}}$	1/Eq	ΔG, (J/mol)	ΔS (J/mol.K)
0 phr	253	0.2833	1.11 x 10^{-4}	4521	--	0.395 x 10^{-2}	-30.914	0.10374
2.5 phr	231	0.3019	1.30 x 10^{-4}	3759	0.9130	0.433 x 10^{-2}	-37.431	0.12561
5 phr	213	0.3200	1.57 x 10^{-4}	3182	0.8403	0.47 x 10^{-2}	-44.715	0.15005
10 phr	204	0.3289	1.71 x 10^{-4}	2931	0.8063	0.49 x 10^{-2}	-48.649	0.16325
15 phr	203.31	0.3297	1.67 x 10^{-4}	2988	0.8143	0.485 x 10^{-2}	-49.015	0.16448

3.6. Variation of Conformational Entropy (ΔS) and Elastic Gibbs free energy (ΔG) of SiR Vulcanizates

To determine the interaction between silicone rubber and Cu-Al-Zn -alloy in the investigated composite the thermodynamic effect were studied. Table3 represents the calculated values of thermodynamic parameters like as ΔG and ΔS. The elastic Gibbs free energy (ΔG) which is estimated from the Flory-Huggins equation as:

$$\Delta G = RT \{\ln (1-Vr) + Vr + \mu\ Vr2\} \quad (9)$$

Where T is the absolute temperature (25 +273k); R is the universal gas constant (8.314 J. mol-1.K-1); μ is the silicone rubber–solvent interaction parameter (0.465) [39] and Vr, which is determined from equilibrium swelling data, is the volume fraction of the silicone rubber matrix in the swelling phase. From the statistical theory of rubber, the elastic Gibbs free energy (ΔG) is related to the conformational entropy (ΔS) of several rubber composites, by the next equation, $-\frac{\Delta G}{T} = \Delta S$, at this point it is expected that there is no variation of interior energy of rubber network during extending [34, 35]. It is evidently renowned from Table 3, that Conformational entropy (ΔS) of SiR 15 phr of Cu-Al-Zn alloy is higher value in comparison to other content of Cu-Al-Zn alloy loading or silicone rubber with filler. The main explanation for the greater value of ΔS in SiR 15 phr of Cu-Al-Zn alloy is the homogeneous dispersion of Cu-Al-Zn alloy inside the rubber matrix. Again, for silicone rubber composites, the value of ΔG is carefully connected to the elastic properties of the composites [15].

Thus, the value of ΔG visibly evidences the greater elastic behavior of SiR/15 phr Cu-Al-Zn -based alloy in comparison to SiR/other alloy loading and SiR without filler. The improved elastic performance of SiR containing 15 phr Cu-Al-Zn based alloy as filler is the result of better compatibility between SiR matrix and alloy. Likewise, ΔG values become more negative as the concentration of Cu-Al-Zn -based alloy increases. On increasing the Cu-Al-Zn -alloy loading, the interfacial area increases up to a certain level due to the decrease in the dispersed phase size by the filler influence [36].

3.7. Scanning electron microscopy (SEM)

The SEM and EDX analysis were performed and presented in Figure 5. It shows that the Cu-Al-Zn -alloy particles are irregular shaped particles with random distribution of the particles and sizes in the range of 9.66-23.62 μm. The Cu-Al-Zn alloy particles showed identifiable peaks between 1.2 and 8 keV of Cu (65.62 wt. %), Al (25.75wt. %) and Zn (8.63 wt. %) as detected by EDX analysis. Cu-Al-Zn alloy predominantly contained Cu, Al and Zn.

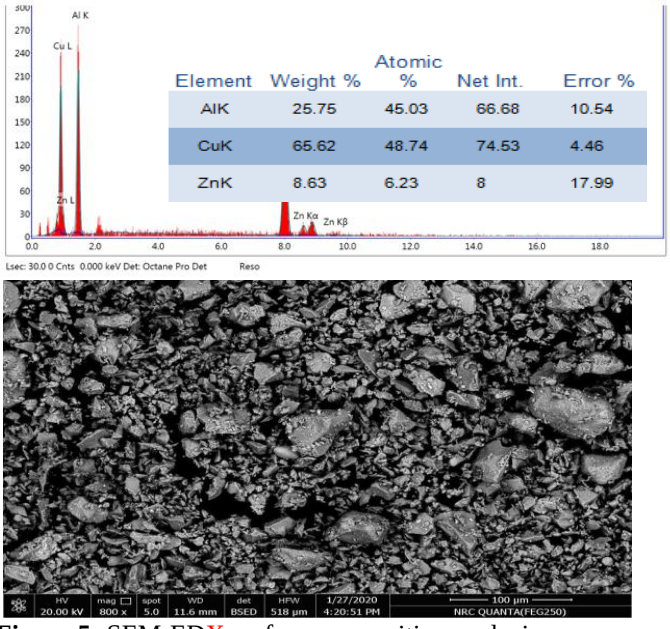

Figure 5: SEM-EDX surface composition analysis of Cu-Al-Zn alloy particles

SEM imaging provides the assessment of the distribution of Cu-Al-Zn alloys into rubber composites and their morpholog. Figure 6 exhibits the fresh fracture surfaces of the Cu-Al-Zn alloy-filled silicone rubber composites. Cu-Al-Zn alloy content at 15 phr provided a uniform filler distribution with small particle sizes, and the fracture surface displayed small holes. The final performance of the matrix will benefit from defects, as well as from a larger interfacial contact area and well-fit uniform dispersion.

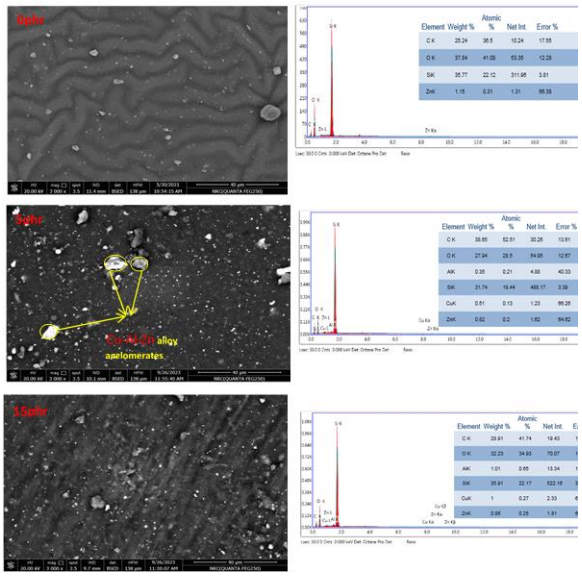

Figure 6: SEM micrographs and EDX spectra Cu-Al-Zn alloy/SiR composites

The Cu-Al-Zn alloy/silicone rubber composite was found to have greater agglomerations of alloy particles at 5 phr. Aggregations of particles will reduce the surfaces of contact throughout silicone rubber and alloy particles, which will subsequently scattering and ultimately lead to a lower thermal resistance. The SiR composite containing 15phr of Cu-Al-Zn alloy displayed less agglomeration than at 5 phr. Such a discovery suggests that Cu-Al-Zn -alloy 15 phr is completely dispersed in the silicone rubber matrix and that there is an interfacial adhesion between the rubber and the alloy, matching the improvement to the mechanical characteristics. The inclusion of Cu-Al-Zn alloy into the silicone rubber matrix is supported by the EDX data [37].

Zn, Si, and O elements are clearly visible in SiR0 as aresult of the EDX examination, showing the existence of ZnO particles (activator). However, the EDX examination revealed the presence of the element Si, which was most likely caused by the electron beam overflowing onto the rubber surface and producing X-rays from the silicone rubber's Si content. The presence of Cu, Al, Zn, Si, and O in the silicone rubber samples containing (5phr, 15phr) proved the inclusion of Cu-Al-Zn alloy in the matrix. The 15phr sample's mineral concentrations were all somewhat higher than those of the 5phr samples.

3.8. Differential scanning calorimeter

Tables 4(a&b) give the specific calorimetric information derived from the DSC curves. As the Cu-Al-Zn alloy loading increased, the peak melting temperatures observed on the second heating scan of the silicone composite phase increased, showing a high degree of SiR crystal perfection. The peak temperature of crystallization recorded on the first heating scan in neat SiR was 173.394°C. The crystallization peak of SiR clearly shifted toward a high temperature in response to the addition of 2.5 or 15 phr of Cu-Al-Zn alloy.

By adding 2.5 or 15 phr of Cu-Al-Zn alloy, the crystallization peak temperature of the composites improved from 173.394 °C to 179.54 °C. The crystallization peak temperature of the 2.5 phr Cu-Al-Zn alloy/SiR composite was higher than that of the 5 phr Cu-Al-Zn alloy/SiR composite, which was lower than that of neat SiR. Defective crystals are a result of silicone's influence on the SiR molecular chains' mobility and rearrangement. In addition, (at second heating scan), the Tm and ΔHm values elevated at introducing 15 phr Cu-Al-Zn alloy accompanied by a drop in the (Tcr) and ΔHcr) values for the crystallization temperature and enthalpies. A decrease in the proportion of amorphous macromolecules can be detected in the shift of the cold crystallization transitions (Tcc) toward a lower temperature range that is observed on all second heating cycles. The addition of treated Cu-Al-Zn alloy decreased the onset temperature (start) while increased the offset temperature. These results confirmed with previous work [7, 8]. The high degree of silicone crystal perfection was detected by DSC and rheological characteristics, which demonstrated that TMSPM was an effective conjunction agent for enhancing Cu-Al-Zn alloy dispersion. The composites physical characteristics demonstrated an increase in stress and strain, a better molecular plane compound, and an increase in energy absorption capacity. It was discovered that the size and shape of the discrete particles are affected by the reality of a join agent (TMSPM). The Cu-Al-Zn alloy particle-SiR matrix interface has been given the TMSPM's approval.

Table 4a: Data derived from the silicone rubber composites' DSC curves (first heating scan).

Cu-Al-Zn alloy content, phr	Tm_a (°C)	ΔHm_a (J/g)	Tcr_a (°C)	ΔHcr_a (m/v)	Tcc_a (°C)	h_a(°C)	$Start_a$ (°C)	$Offset_a$ (°C)	Tga(°C)
0 phr	215.16	66.234	173.394	2.069	150.01	150	189.32	187.03	-125
2.5 phr	203.38	36.409	179.54	1.503	140.17	140.17	140.46	193.37	-127.2
5 phr	167.01	5.678	153.668	0.523	133.36	133.4	136.673	159.317	-128.7
10 phr	205.64	30.576	168.166	2.281	122.68	122.7	125	204.908	-132.6
15 phr	198.99	8.187	179.688	0.682	155.03	155.03	155.224	195.34	-136.7

h_a is the first heating scan, and h_b is the second heating scan, *Tm**a*** is the melting temperature recorded on the first heating scan, *Tm**b*** is the melting temperature recorded on the second heating scan, ***Tcr*** is the crystallization temperature, ***Tcc*** is the cold crystallization temperature, *ΔHma* is the enthalpy of the melting profile recorded on the first heating scan, *ΔHm**b*** is the enthalpy of the melting profile recorded on the second heating scan, and *ΔHcr* is the crystallization enthalpy

Table 4b: Data derived from the silicone rubber composites' DSC curves (second heating scan).

Cu-Al-Zn alloy content, phr	Tm_b (°C)	ΔHm_b (J/g)	Tcr_b (°C)	ΔHcr_b (m/v)	Tcc_b (°C)	h_b (°C)	$Start_b$ (°C)	$Offset_b$ (°C)	Tga(°C)
0 phr	--	---	---	---	----	---	---	---	-125
2.5 phr	589.2	4.473	585.789	-1.96	580.89	580.9	583.639	588.105	-127.2
5 phr	592.5	3.645	592.5	- 0.653	578.37	578.4	580.458	589.852	-128.7
10 phr	607.34	10.006	580.723	-1.362	554.58	554.6	563.44	590	-132.6
15 phr	599.77	14.149	583.614	-2.066	571.19	571.2	573.99	595.255	-136.7

3.9. Dielectric Properties of treated Cu-Al-Zn alloy/SiR composites

The permittivity ε' of SiR slightly decreases as frequency increases Figure. 7. This is true for the blank sample and up to 2.5phr of metal alloy (treated Cu-Al-Zn alloy). At minor frequencies, all allowed dipolar collections can exchange and thus produce a high ε' whereas at high, these groups fight to move, causing a reduction in permittivity ε'. For the higher loading composites, the permittivity of the samples containing (5phr- 15phr) of treated Cu-Al-Zn alloy tends to sharply increase at lower frequencies. This increase is probable referred to the existence of a noteworthy volume fraction of the metal alloy (treated Cu-Al-Zn alloy) at the interfaces and may subsequently cause an increment in the accumulation of charges and consequently increase interfacial polarization that in turn produces higher permittivity [38].

The permittivity ε' increases as the loading of Cu-Al-Zn alloy, increased as shown in Figure 8a. Conversely, in the low-frequency range, the dielectric loss ε" was mostly attributed to the lag in interfacial polarization, which was caused by charge carrier movement and trapping at the interfacial area. When comparing the response times of the other three types of polarization, the interfacial polarization type has a significantly long response time. The majority of the energy resulting from the delay in interfacial polarization was converted into thermal energy released into the atmosphere, which was detected as dielectric loss. There was also a noticeable loss peak in the high-frequency range (around 1 MHz). This peak was ascribed to the rubber's chain segmental motion and the orientation polarization's latency. Before this range of frequencies, the orientation polarization can match. Prior to this frequency region, the orientation polarization can keep up with the change in electric field completely. Also, the dielectric loss ε" increases with the increase of treated Cu-Al-Zn alloy Figure 8b.

Moreover, electrical conductivity σ as a function of treated Cu-Al-Zn alloy concentration is presented in Figure 8c. An improvement in the electrical performance of SiR is noticed by increasing metal Cu-Al-Zn alloy loading. Nonetheless, the development of a three-dimensional network of particles within the matrix is a prerequisite for SiR composites' electrical conductivity. The electrical performance is the result of two primary mechanisms [39, 40]. Since electrons can move from one particle to another, direct particle interaction presents the easiest scenario; the tunnel effect is the second mechanism. When two particles are separated by a tiny layer of polymer, this happens. Besides, the particle concentration plays a dominant role, for example, a high particle concentration should allow the formation of the three dimensional network. As shown in Figure 8c, when the treated Cu-Al-Zn alloy concentration in the composite reached 5 phr, conductivity increased significantly. This abrupt increase in electrical conductivity resulted from treated Cu-Al-Zn alloy in the elastomer matrix forming a continuous network.

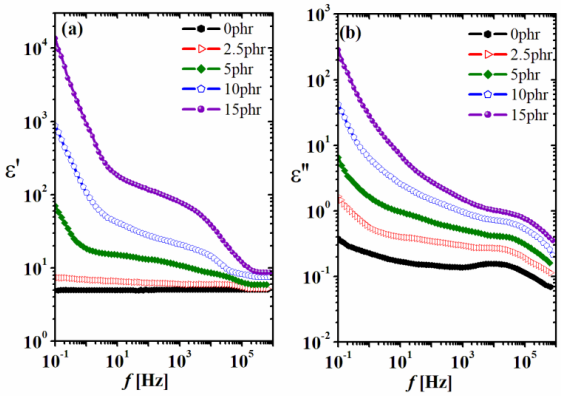

Figure 7: The variation of permittivity ε′ and dielectric loss ε" with frequency *f* at 30oC for SiR / Cu-Al-Zn alloy.

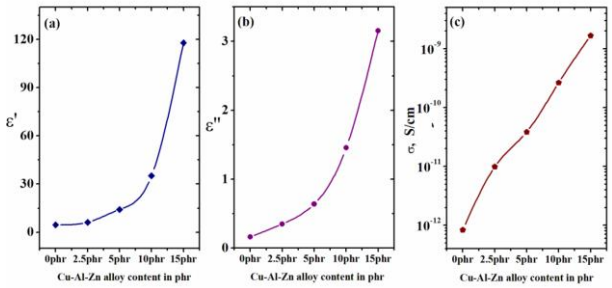

Figure 8: The dependence of permittivity ε′ and dielectric loss ε" and electrical conductivity σ on treated Cu-Al-Zn alloy content

4. Conclusion

- Cu-Al-Zn based alloy/SiR composites were successfully produced. Silicone rubber (SiR) was combined with various concentrations of treated Cu-Al-Zn alloy at 2.5, 5, 10, and 15 phr.

- The swelling performance was enhanced with higher loading of Cu-Al-Zn -based alloy. It has been noted that the values of volume fraction (Vr) of SiR/ Cu-Al-Zn -alloy composites are higher than those without. Likewise, the equilibrium swelling reduced with increased Cu-Al-Zn -based alloy loading.
- The examined silicone rubber composites showed improved physical properties (mechanical and rheometric properties) as a result of the homogeneous diffusion of Cu-AL-Zn alloy particles (15phr) in the presence of the coupling agent (TMSPM). The SiR composites, which includes 15 phr Cu-Al-Zn alloy and had stress of 6.84 MPa and strain at break of 1107%, was considered to be the best sample for further testing.
- The value of ΔG indicates that SiR/15 Cu-Al-Zn alloy has greater elastic behavior in comparison to SiR without alloy as ΔG is is closely related to the material's elastic behavior. The superior elasticity of SiR/15phr Cu-Al-Zn alloy is described by obtaining better compatibility between silicone rubber matrix and Cu-Al-Zn based alloy.
- The permittivity (ε′) values increased by incorporating Cu-Al-Zn alloy. Additionally, the Si R composites containing Cu-Al-Zn alloy show promising insulation properties and can be employed for electrical insulation needs.

5. Conflicts of interest

The authors declare that the article content has no conflict of interest.

6. Acknowledgments

The present work is supported through the National Research Centre Project No. 12010313.

7. References

[1] Bhaskar, J., Sharma, A.K., Bhattacharya, B., Adikari, S. (2020). A review on shape memory alloy reinforced polymer composite materials and structures. Smart Materials and Structures, 29073001(25PP).

[2] Wei, Z.G., Sandstrom, R., Miyazaki, S. (1998). Review shape memory materials and hybrid composites for smart systems. Journal of Materials Science, 333743-3762.

[3] Oliveira, J.P., Zeng, Z., Zhou, T., Miranda, R., Braz Fernandes F.M. (2016). Improvement of damping properties in laser processed superelastic Cu-AL-Mn shape memory alloys. Materials and design, 98, 280-284.

[4] Adupa, S., Pulla, S., Alavala, C.R. (2021). Effect of filler materials in silicon rubber for the electrical insulation applications: A Review. International Journal of Applied Engineering Research, 16, 721-729.

[5] Heller, L., Vokoun, D., Finckh, P.S. (2012). An original architecture NiTi silicon rubber structure for biomedical applications. Smart Materials and Structures, 21045016.

[6] Reghunadhan, A., Paduvilan, K., Vayyaprontavid, A., Prajitha, K., Michal, V.S., Thomas, S. (2021). Shape memory materials from rubber. Materials, doi.org/10.3390.

[7] Rodino, S., Curcio, E.M., Renzo, D.A., Sgambitteraa, E., Magaro, P., Furgiuele, F., Brandizzi, M., Maletta, C. (2022). Shape memory alloy- polymer compsites: static and fatigue pullout strength under thermo-mechanical loading. Materials, doi.org/10.3390.

[8] Vijayalekshmi, V., Abdul Majeed, S.S.M. (2013). Mechanical, thermal and electrical properties of pdm/silicone blend nanocomposites. International Journal of Engineering Research and Applications, 3, 1177-1180.

[9] Raja Prabu, R., Usa, S., Udayakumar, K., Abdul Majeed, S.S.M, Abdullah Khan, M. (2007). Electrical insulation characteristics of silicone and EPDM polymeric blends-Part I. IEEE Transactions on Dielectrics and Electrical insulation, 14, 1207-1214.

[10] Mackevich, J., Shah, M. (1997). Polymer outdoor insulating materials Part-I: comparison of porcelain and polymer electrical insulation. IEEE Electrical insulation magazine, 13, 5-10.

[11] Simmons, S., Mackevich, J., Shah, M., Chang, R.J. (1997). Polymer outdoor insulating materials Part-III: Silicone Elastomer considerations. IEEE Electrical insulation magazine, 13, 25-32.

[12] Ehsani, M., Borsi, H., Gockenbach, E., Bakhshandeh, G.R, Morshedian, J., Abedi, N. (2004). Study of Electrical, dynamic mechanicaland surface properties of silicone-EPDM blends. IEEE International conference on solid dielectrics, 5-9.

[13] Cherney, E.A. (2005). Silicone rubber dielectrics modified by inorganic fillers for outdoor high voltage insulation applications. IEEE Transactions on Dielectrics and Electrical Insulation, 12, 1108-1115.

[14] Janowska, G., Jastrzabek, A.K., Rybinski, P. (2011). Thermal stability, flammability and fire hazard of butadiene-acrylonitrile rubber nanocomposites. Journal of Thermal Analysis Calorim, 103, 1046.

[15] Mahmoud, D.S., El-Sabbagh, S.H., El-Basheer, T.M., Moustafa, A.M., Barakat, M.A.Y. (2023). Rheometeric, ultrasonic and acoustical shielding properties of Cu-alloy/silicone rubber composites for electronic applications. Journal of Thermoplastic Composite Materials, 1-23, DOI: 10.1177/08927057231162016.

[16] Barakat, M.A.Y., El-Sabbagh, S.H., Mohamed, W.S., Mahmoud, D.S. (23023. Nanoarchitectonics of ethylene propylene diene monomer (EPDM) composites reinforced with Cu–Al–Zn alloy for ultrasonic array transducers' fabrication. Applied Physics A, 129:422, https://doi.org/10.1007/s00339-023-06688-w.

[17] Nassar, A., Mahmoud, D.S., Mohamed, W.S., Moustafa, A.M., El-Sabbagh, S.H. (2021). Investigation of the structure, magnetic, rheological and mechanical properties of EPDM rubber/Cu-Al-Zn alloy composites. Egyptian Journal of Chemistry, 64, 7277-7291.

[18] Rivlin, R.S., Thomas, A.G. (1953). Rupture of rubber. I. Characteristic energy for tearing. Journal of Polymer Science, 10, 291-318.

[19] El-Sabbagh, S.H., Ahmed, N.M., Turky, G.M., Selim, M.M. (2017). Rubber nanocomposites with new core-shell metal oxides as nanofillers Ch. In Progress in Rubber Nanocomposites. In Progress in Rubber Nanocomposites. Edited by Sabu Thomas Hanna J. Maria, Woodhead Publishing is an imprint of Elsevier, pp. 249–283.

[20] Wang, J., Chen, D. (2013). Mechanical properties of natural rubber nanocomposites filled with thermally treated attapulgite. Journal of Nanomaterials, 11, 496584,

[21] Nabil, H., Ismail, H., Azura, A.R.(2013). Compounding, mechanical and morphological properties of carbon-black-filled natural rubber/recycled ethylene-propylene-dienemonomer (NR/R-EPDM) blends. Polymer Testing, 32, 385-393.
[22] Lee, B.L. (1979). Reinforcement of uncured and cured rubber composites and its relationship to dispersive mixing an interpretation of cure meter rheographs of carbon black loaded SBR and cis-polybutadiene compounds. Rubber Chemistry and Technology, 52, 1019-1029.
[23] Nassar, A., Yehia, A.A., El-Sabbagh, S.H. (2015). Evaluation of the physico-mechanical and electrical properties of styrene-butadiene rubber/aluminum powder and styrene-butadiene rubber/cerium sulfate composites. POLIMERY, 60, 100-108.
[24] Abdelsalam, A.A., Araby, S., El-Sabbagh, S.H., Abdelmoneim, A, Hassan, M.A. (2021). Effect of carbon black loading on mechanical and rheological properties of natural rubber/ styrene-butadiene rubber/ nitrile butadiene rubber blends. Journal of Thermoplastic Composite Materials, 34, 490-507.
[25] Othman, H.S., El-Sabbagh, S.H., Nawwar, G.A. (2022). Utility of copper (lignin/silica/fatty acids) complex derived from rice straw as antioxidant/hardening and fluid resistant agent in nitrile-butadiene rubber composites (PART IV). Pigment and Resin Technology, 51, 518-527.
[26] Khalaf, A.I., Ward, A.A., Abd El-Kader, A.E., El-Sabbagh, S.H. (2015). Effect of selected vegetable oils on the properties of acrylonitrile-butadiene rubber vulcanizates. POLIMERY, 60, 43-56.
[27] Mahmoud, W.E., Mansour, S.A., Hafez, M., Salam, M.A. (2007). On the degradation and stability of high abrasion furnace black (HAF)/acrylonitrile butadiene rubber (NBR) and high abrasion furnace black (HAF)/graphite/acrylonitrile butadiene rubber (NBR) under cyclic stress-strain. Polymer Degradation and Stability, 92, 2011-2015.
[28] Lorenz, O., Parks, C.R. (1961). The crosslinking efficiency of some vulcanizing agent in natural rubber. Journal of Polymer Science, 50, 299.
[29] Ahmed, N.M., El-Sabbagh, S.H.(2011). The influence of hybrid phosphate–alumina pigments on properties of Ethylene-propylene-diene rubber composites. Materials and Design, 32, 303-321.
[30] Morsi, S.M.M., Mohamed, H.A., El-Sabbagh, S.H. (2019). Polyesteramidesulfone as novel reinforcement and antioxidant nanfiller for NBR blended with reclaimed natural rubber. Materials Chemistry and Physics, 224, 206-216.
[31] Mahmoud, D.S., Said, A.A, Abd El-Kader, A.E., El-Sabbagh, S.H. (2022). Enhanced physicomechanical performance of nitrile rubber composites by utilizing eco-friendly natural oil as a plasticizer. Journal of Vinyl and Additive Technology, 28, 894-906.
[32] El-Nemr, K.F., Hassan, M.M., Saad, E.A., Hamdy, E. M. (2017). Reinforcement of acrylonitrile butadiene rubber with waste rubber ash using ionizing radiation. Journal of Vinyl and Additive Technology. 23, 117-124.
[33] Roy, k., Alam, M.N., Mandal, S.K., Debnath, S.C. (2015). Silica-coated nano calcium carbonate reinforced polychloroprene rubber nanocomposites: influence of silica coating on cure, mechanical and thermal properties. Journal of Nanostructure in Chemistry, DOI 10.1007/s40097-015-0174-x.
[34] Roy, k., Alam, M.N., Mandal, S.K., Debnath, S.C. (2015). Preparation of zinc-oxide-free natural rubber nanocomposites using nanostructured magnesium oxide as cure activator. Journal of Applied Polymer Science, 42705, 1-7.
[35] Xiangyu, W., Jing, Z., Rui, M., Yu, Z., Weihong, G. (2022). Preparation and properties of room-temperature-vulcanized silicone rubber using modified dopamine as a crosslinking agent. Materials Research Express, 9, 1-13.
[36] Jovanovi, S., Samarzˇija-Jovanovi, S., Markovi, G., Jovanovi, V., Adamovi, T., Marinovic´-Cincovic´, M. (2018). Ternary NR/BR/SBR rubbers blend nanocomposites" Journal of Thermoplastic Composite Materials, 31, 265-287.
[37] Jiaying, Q., Lu, F., Jean, F.M., Cui, L., Yu, C. (2021) A silicon rubber composite with enhanced thermal conductivity and mechanical properties based on nanodiamond and boron nitride fillers. Polymer Composites, 42, 4390-4396.
[38] Saied, M.A., Ward, A. A. (2020). Physical, dielectric and biodegradation studies of PVC/silica nanocomposites based on traditional and environmentally friendly plasticizers. Advances in Natural Sciences: Nanoscience and Nanotechnology, 11 035003.
[39] Gojny, F.H., Wichmann, M.H.M, Fiedler, B., Kinloch, I.A., Bauhofer, W., Windle, A.H., Schulte, K. (2006). Evaluation and identification of electrical and thermal conduction mechanisms in carbon nanotube/epoxy composites. Polymer, 47, 2036-2045.
[40] Ward, A.A, Stoll, B., Von, S.W., Herminghaus, S., Bishai, A.M., Hanna, F.F. (2003). Studies on the dielectric behavior of silica-filled butyl rubber vulcanizates after cyclic deformation Journal of Macromolecular Science, 42, 1265-1280

.